Exciting passive dynamics in a versatile bipedal robot

Daniel Renjewski*, Alexander Spröwitz, and Jonathan Hurst

Dynamic bipedal robots, which are capable of versatile behaviour, are rare. Most bipedal robots are either versatile and static or dynamic and limited to specific gaits. Over the last twenty years the bio-inspired spring mass model became a versatile template for bipedal walking and running gaits with many studies motivated by its high potential for versatile robot locomotion. However the characteristic dynamics have not yet been demonstrated with human size robots.

We show that we can reproduce the dynamics of this versatile template for locomotion in a human-size biped utilizing its specifically designed natural dynamics. Spring mass walking with characteristic double humped force profiles is demonstrated over a range of speeds. Using the same controller, the robot exhibits grounded running, walks over steps, and in an natural outdoor environment.

The robot is an important step towards bipedal machines capable to compete with animals in terms of efficiency, robustness and versatility and enables a better understanding of fundamental biological movement principles.

***Index Terms*—passive dynamics, robot control, humanoid robots, legged locomotion**

I. Introduction

Walking and running animals are inherently energy economic, agile and versatile. Natural locomotion with its impressive dynamics relies on structural leg compliance for the physical interaction with the environment [1]. The Spring-Mass template model is the only reduced-order model that reproduces the basic dynamics of human and animal walking and running, including ground reaction forces and energy cycles. We claim that designing the desired spring-mass passive dynamics into a machine enables the versatile and agile behaviors observed in animals. In this paper, we demonstrate some basic theoretically-predicted gaits on *ATRIAS* (**A**ssume **T**he **R**obot **I**s **A** **S**phere), a spring-mass, human-scale, bipedal robot.

The complexity of natural locomotion neuromechanics gave rise to reductionist models to identify basic locomotion principles. Attempts were made to capture natural dynamics of walking with models almost as simple as a rolling wheel [2]. The spring mass template originally proposed for running [3] was found to better resemble the oscillatory nature of bipedal walking [4] exhibiting feasible walking gaits over a wide parameter range. The model has been widely investigated for its dynamic properties [5]–[8] and its capabilities to reproduce human walking and running [9], [10]. A number of control strategies have been proposed in simulation studies, primarily for running [11]–[14], but despite the frequently stressed relevance for robotics, matching natural locomotion with technical devices is an ongoing challenge.

In robotics, compliance is not commonly used in bipedal machines as it complicates control by introducing additional, non-actuated degrees of freedom. Rigid robots of two design classes cluster at opposite ends of a spectrum spanning from versatile to efficient. One end is occupied by highly economical, underactuated bipedal robots utilizing their natural dynamics passively which limits them to few, very specific gaits [15]–[18]. On the other end, fully actuated advanced humanoids are capable of versatile locomotion, e.g. Asimo [19], Toyotas Humanoid [20] or HRP [21], but exhibit rather static, inefficient gaits. We see little hope that either design approach can combine versatility and efficiency as observed in natural locomotion.

Only few robots have actually implemented passive mechanical compliance in their legs to enable force control [22], [23] or due to a biomimetic design approach [24]–[27]. To our knowledge resulting locomotor dynamics from experiments with robots have only been reported in [28]. Ground reaction forces as exhibited by the spring mass model for walking and running that represents animal locomotion has, to our knowledge, not been demonstrated in robots before.

The bipedal robot *ATRIAS* was designed based on the physics of the spring-mass model to resemble its dynamics (Figure 1) and to test theoretically proposed control strategies. We demonstrate, that desired passive dynamics can be engineered into versatile robots. The robustness with regard to changing locomotion speed, gait types and environmental conditions as predicted by the template is demonstrated on the robot. The experimental results we present confirm the robots ability to exhibit spring-mass-model dynamics and robust locomotor behaviour.

The following section describes the experimental methods used including the robot and experiment setup, controllers as well as data acquisition and processing. Section III describes the experimental results. In Section IV we discuss the implications of our results for robot design and control as well as for investigating locomotion in nature.

We conclude that spring-mass walking can meet its theoretical potential on real systems. We demonstrate a variety of dynamic walking gaits, robust to the environment, and energy economic, enabled by template-driven machine design, and a controller that excites the passive dynamics.

Daniel Renjewski and Jonathan Hurst are with the Dynamic Robotics Laboratory, School of Mechanical, Industrial and Manufacturing Engineering, Oregon State University, 021 Covell Hall, Corvallis, Oregon 97331, USA.

Alexander Spröwitz is with the Structure & Motion Laboratory, The Royal Veterinary College, Hawkshead Lane, North Mymms, Hatfield, Herts AL9 7TA, UK.

*corresponding author, who can be reached at daniel@human-motion-engineering.org

Nomenclature							
σ	Sample	x	Horizontal position	F_{tan}	Tangential leg force	φ_{As}	Segment angle A
t	Time	y	Vertical position	k	Spring stiffness	φ_{Bs}	Segment angle B
m	Mass	CoM	Center of mass	$\tilde{v}$	Average velocity	φ_{Am}	Motor angle A
v	Velocity	CoT	Cost of transport	F_r	Froude number	φ_{Bm}	Motor angle B
P	Power	GRF	Ground reaction force	I_m	Motor current	φ_{md}	Desired motor angle
l	Leg length	LTP	Lowest turning point	k_p	Proportional gain	$\dot{\varphi}$	Angular velocity
F_{ax}	Leg force	F_x	Horizontal force	k_d	Derivative gain	φ_{AEA}	Anterior extreme angle
τ	Torque	F_y	Vertical force	g	Gravitational acceleration	φ_{PEA}	Posterior extreme angle
U	Voltage	s	Segment length	κ	Rotational spring stiffness	φ_l	Leg angle

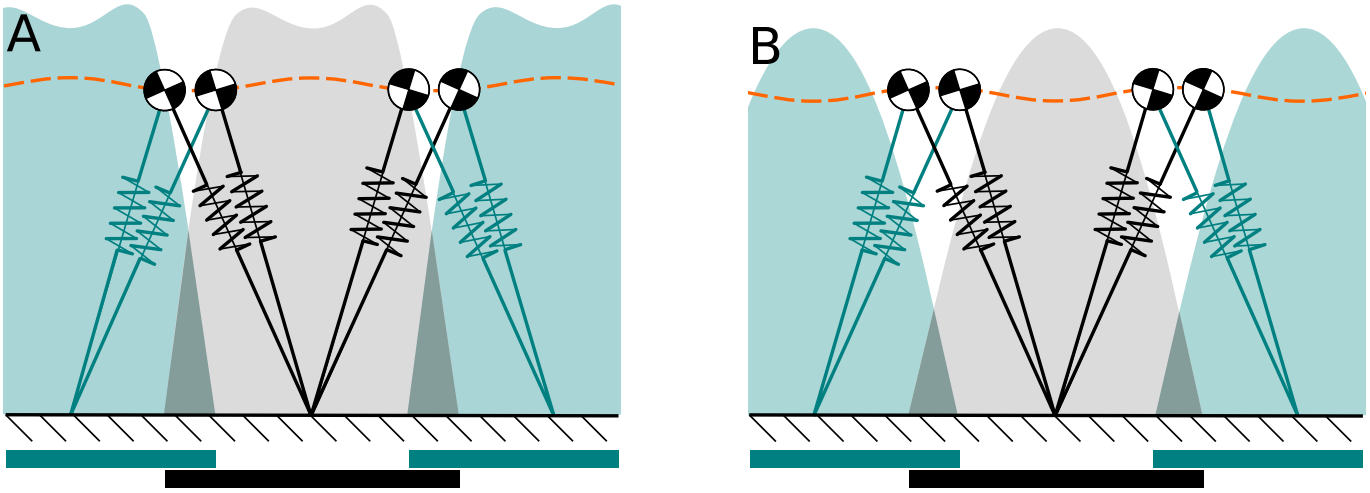

Fig. 1: Schematic representation of the center of mass (CoM) dynamics of a walking gait (A), and a grounded running gait (B). **A)** The CoM (black and white circle) of a walking human or animal describes an oscillating motion (dashed orange line) with a maximum around mid-stance. Four instants of leg transition (two for the swing leg touching down and two for the stance leg taking-off) are shown. The smooth oscillation through the lowest turning point (LTP) during the distinct double support phase, while transitioning support from one leg (green) to the other (black), are key characteristics of compliant walking. The double support phase is emphasized by horizontal bars indicating ground contact of the respective leg. The vertical ground reaction forces (GRF, shaded background areas) show a double-peak profile during the leg's stance phase. **B)** For grounded running, a single-peak, GRF is visible, somewhat similar to the force profile of running (not shown). However, double leg support phases exist and no aerial phases occur. The CoM shows a minimum around mid-stance, and an out of phase motion with the CoM. Experimental GRF and CoM motion plots of the *ATRIAS* robot corresponding to these two gaits can be found in Fig. 7 and Fig. 9. Figure modified from [29].

II. Methods

In our experiments, we tested the robot in a controlled experimental setup for its capabilities to utilise its natural leg compliance to generate compliant gaits.

A. Robot background

All experiments were executed on the bipedal robot *ATRIAS*, a machine of 1.70 m height and 60 kg weight. The mass of the robot is concentrated in the trunk, one leg accounts for about 5 % of the total weight. Six motors power the robot, two in parallel on each leg and one for each hip. The *ATRIAS* robot neglects the morphology of biological legs to implement the dynamic functionality of a compliant leg as proposed by the spring mass model for walking and running. A four-bar mechanism gears the dynamic interaction between two parallel series elastic actuators (SEA) and the supporting substrate (Fig. 2). Although the leaf springs of the SEAs have a nearly linear torque-angle relation (κ), the linkage system induces a nonlinear spring stiffness for the entire leg (k). The motors attached to each spring (MF0150010-X0X, Allied Motor Technologies, Tulsa, OK, USA) are rated for 532 W continuous power, geared with a 50:1 harmonic drive and deliver a theoretical stall torque of 300 Nm at the gear output end. Four 32-bit optical encoders (RL32BAT001B30F, Renishaw, Wotton-under-Edge, UK) measure the motor positions φ_{Am} and φ_{Bm} and the segment positions φ_{Al} and φ_{Bl} relative to the trunk's anteroposterior axis (Fig. 2). Based on measured angles, robot states such as leg angle, spring deflection and leg forces were calculated (Tab. I). More

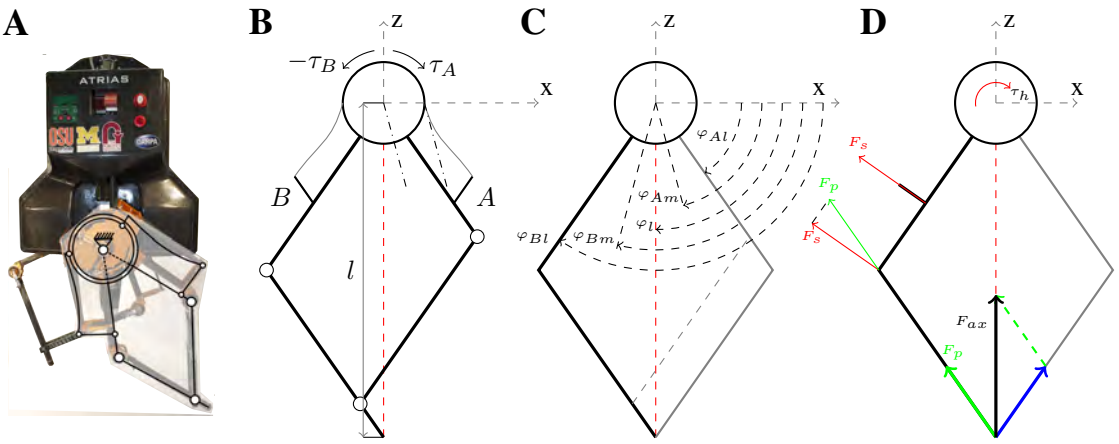

Fig. 2: Schematic representation of *ATRIAS*' leg geometry, and force transmission. **A)** Schematic abstraction of the mechanical leg design: **B)** Four-bar leg mechanism (thick lines) and attached springs (thin lines) connected to separate motors: motor A and motor B. Dash-dotted lines indicate the angle at the motor output projected to the hip joint. The virtual leg is indicated by the red dashed line. **C)** Angle definitions: φ_{Al} – side A segment angle, φ_{As} – side A motor angle, φ_l – virtual leg angle, φ_{Bs} – side B segment angle, φ_{Bm} – side B motor angle; **D)** Force projection: F_s – spring reaction force on spring attachment and projected onto joint, F_p – spring reaction force projected on lower segment, F_{ax} – reaction force along leg axis resulting from spring deflections of spring A and spring B.

technical details are available in [30]. The robot's CoM is located approximately 12 cm above the hip joint and for the small weight of the segments in motion does not move much itself. Therefore, the trunk's position is a good representation of the CoM and the virtual leg and axial forces correspond to the respective properties of the spring mass model.

Like any other physical system, this robot did not operate in an energy conserving manner. Mechanical energy has been dissipated, for example through friction and non-elastic collisions. To restore dissipated mechanical energy, hip torques were generated. These result in tangential leg forces, which are not present in the standard energy conservative template model.

Virtual leg angle	$\varphi_l = \frac{\varphi_{Bs}+\varphi_{As}}{2}$
Virtual leg length	$l = 2 \cdot s \cdot cos(\varphi_l - \varphi_{Al})$
Spring deflection A	$\varphi_{As} = \varphi_{Am} - \varphi_{As}$
Spring deflection B	$\varphi_{Bs} = \varphi_{Bm} - \varphi_{Bs}$
Leg spring stiffness	$k = \frac{\kappa}{2s^2}(\frac{\chi - \frac{l}{2s}\cdot(acos(\frac{l}{2s}) - acos(\frac{l_0}{2s}))}{\chi^3})$
	$\chi = \sqrt{(1-(\frac{l}{2s})^2)}$
Axial leg force	$F_{ax} = \frac{\kappa}{2s} \cdot (\frac{\varphi_{Am}}{sin(\varphi_{As}-\varphi_l)} + \frac{\varphi_{Bm}}{sin(\varphi_l - \varphi_{Bs})})$
Hip torque	$\tau_h = \tau_A + \tau_B$
Tangential leg force	$F_{tan} = \tau_h \cdot l$

TABLE I: Derived kinematic and dynamic robot states.

Fig. 3: Experimental setup: robot mounted to the boom, remote control computer and graphical user interface visible in the top left corner. When operating, the robot was always carrying its own weight. The suspension only acted as a fail-safe, and was carefully adjusted to stay slack during experimental operation.

B. Experimental setup

Three types of experiments were executed: (**E1**) steady gait experiments in a laboratory environment, on flat ground, (**E2**) step down experiments onto flat ground and (**E3**) steady gait experiments in a natural environment.

The experimental setup consisted of the robot attached to a boom restricting the robot's motion to its saggital plane while moving on a circular track [31]. For all flat ground experiments the ground was covered with rubber mats. The boom was fixedly attached to the trunk and constrained pitch.

Encoders on the boom measured its horizontal and vertical displacement. To minimize unintended interference during the experiments, the boom was designed with low rotational inertia and rotational friction.

For the **(E2)** trials a set of steps was constructed to elevate the robot above level ground. The resulting drop had a height of 7.8 cm (8.6 % leg length). The controller has not been modified nor was the obstacle sensed by the robot. The control parameters are listed in Tab. II.

(E3) experiments were executed on a natural lawn, where the boom was placed and suspended from a tree. The surface was irregular and differed in structure and compliance. No modifications have been made to the robot's mechanics or the controller.

C. Control

Two main tasks had to be addressed by the controller – facilitate the robot to walk with minimally affecting its passive dynamics and recirculating the leg during swing. The challenges were to ensure sufficient support and propulsion continuously and developing a strategy for leg swing. To enable the robot's passive dynamics, only the motor position was used for control allowing the springs to deflect freely depending on the physical interaction of the robot with the ground. The controller (Fig. 4) is an adapted version of the equilibrium point controller used in [28]. Phase driven swing leg control is an extension of the concepts proposed in [32] and [33].

This controller ensures that the key functions of locomotion, i.e. support and propel the body, are achieved. In order to maintain support, a reference position of the motors is calculated based on the current leg angle and a desired leg length assuming no spring deflection. The deviation of the current motor position from the desired motor position is used to calculate motor currents (Eq. 2). The motor current for motor B is than offset by a constant value to generate a hip torque (Eq. 3).

In contrast to the spring mass model, leg recirculation has to be facilitated by active control serving a number of objectives: sufficient ground clearance to prevent tripping, smooth transitioning from stance into flight and vice versa, as well as timely completion. For motion timing a virtual constraint is introduced to tie the swing leg motion to the stance leg motion [34].

Transitioning and phasing of the two legs are critical for successful walking. A state machine is controlling the assignment of stance and flight leg and transitions based on the virtual constraint when the stance leg reaches the predefined posterior extreme angle.

Stance phase: Keeping the center of mass (CoM) sufficiently high above the ground is a fundamental task of legged locomotion. Both motors of the stance leg were commanded to maintain a constant angular deviation from each other that corresponds to a desired leg length not considering any spring deflection. This angle was centered off the current virtual leg angle as calculated based on sensor readings (Table I).

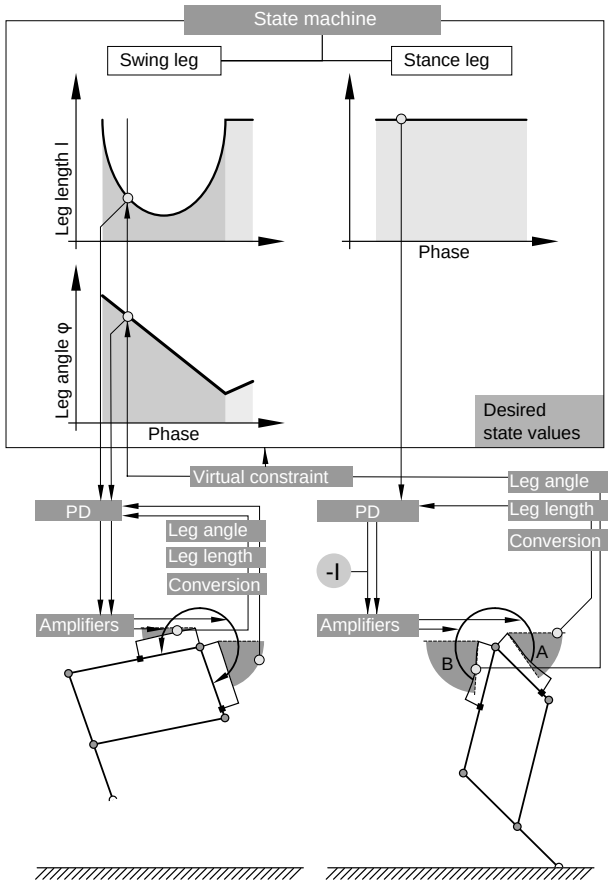

Fig. 4: Schematic presentation of the controller implemented for experiments with the *ATRIAS* robot. A state machine triggers the transition from stance to swing, and from swing to stance when the stance leg reaches its preprogrammed posterior extreme angle (AEA). The motors are kept at a constant angle from each other representing a desired leg length without spring deflection. A current offset for one motor induces a hip torque. The phase of the stance leg drives desired leg length l and desired leg angle φ of the flight leg which are fed into a PD controller that generates the required swing leg motor current commands. During the first part of swing phase, the leg is protracting (dark grey background). At the end of swing phase, the leg is retracting, before it reaches touch-down (swing leg retraction, light grey background).

Deviations from desired motor angles (φ_{md}, Eq. 1) were corrected by PD control, which generated the motor control signal in terms of motor current (I_m, Eq. 2).

$$\varphi_{md} = \varphi_l \pm acos(\frac{l}{2s}) \tag{1}$$

$$I_m = k_p \cdot (\varphi - \varphi_{md}) + k_d \cdot (\dot{\varphi}), \tag{2}$$

where φ denotes the desired position. The reference to the current leg angle preserved the leg's momentum rotating posteriorly. To account for losses of mechanical energy an additional hip torque was induced by reducing the commanded current of the posterior motor (B) by a constant amount (I_τ,

Eq. 3).

$$I_{mB} = I_m - I_\tau \tag{3}$$

Flight phase: Leg recirculation consisted of three phases enabled by piecewise, phase-based functions (Fig. 4): transition from stance into flight, bringing the leg into an anterior position, and transition into stance. The timing of these phases was based on a virtual constraint (c_v, Eq. 4) related to the virtual stance leg angle (φ_l). The timing was controlled such that the swinging leg reached the desired touch down position when the stance leg reached its desired posterior extreme angle.

$$c_v = 1 - \frac{\varphi_{pea} - \varphi_l}{\varphi_{pea} - \varphi_{aea}} \tag{4}$$

During the first phase the kinematic chain with both feet on the ground had to be resolved such that no constraining forces impeded the gait. Therefore the posterior motor was commanded to keep the deflection of spring B smaller than the deflection of spring A ($\varphi_{Bs} < \varphi_{As}$) while both motors shortened the leg. The leg then followed a predetermined, hyperbolic trajectory parametrised with respect to the virtual constraint using PD control on swing leg position based on motor orientation. Due to the lightweight nature of the distal segments, the spring dynamics could be neglected during flight. This brought the leg to an anterior position, first compressing then extending it to its full length (Fig. 6). In final swing, the leg was retracted toward touch down. As soon as the now trailing stance leg reached the predetermined posterior extreme angle the legs state machine transitioned the leg assignments and the leading leg gradually took over body support. This resulted in a double support phase, when both legs were in contact with the ground at the same time until the trailing leg broke contact.
The controller had been implemented in *C++* and was executed at a 1 kHz control rate on an onboard computer. Control parameters were altered remotely using a graphical user interface. A detailed description of the electronics and control system can be found in [35].

D. Experiments

The series of **(E1)** experiments aimed at investigating **i)** the capability to control series compliant legs to generate steady walking, **ii)** quantifying the achieved gaits in terms of dynamics and energetics and **iii)** assessing the robot's morphology and actuation for their suitability to generate dynamic bipedal locomotion. Experiments of type **(E2)** and **(E3)** were conducted to assess the robot's potential to cope with uneven terrain for future controller extensions.
Experiments were carried out to test a number of different control parameters generating walking gaits at different speeds. At the beginning of each experiment a number of control parameters where altered, mostly affecting step length and hip torque (Tab. II). All parameters were determined experimentally.
Each experiment started with the robot suspended in the air. When the motors were powered and the robot enabled, *ATRIAS* initialised to a default position before being lowered onto the ground until it supported itself. Initially the robot was standing supported by both legs, one leg at its predefined anterior extreme angle (φ_{AEA}) and one at the posterior extreme angle (φ_{PEA}). The gait was then initiated by manually triggering a phase switch operating the leading leg as stance leg and the trailing leg as swing leg. The hip torque retracted the stance leg and accelerated the robot into a walking gait. For all reported experiments, the robot achieved a nominal forward speed and settled into a steady gait after a few steps.
For outdoor experiments the entire experimental setup including the supporting boom was moved outdoors (Figure 11).
Data of the robot motion has been recorded at 1 kHz. All data has been synchronised and checked for timing errors. Kinematic and dynamic time-series were calculated based on recorded sensor data(Tab. I).

E. Data processing

Sensor data of the robot has been recorded and processed for use in Matlab (2012b, The Mathworks, Natick, MA, USA). Electrical and mechanical power and cost of transport were calculated from experimental data. Sensors measured the current (HASS 50-S, LEM USA Inc., Milwaukee, WI, USA) through the robot's power supply cables and the supply voltage. The voltage signal was filtered using a single pole recursive low-pass filter. For comparability three steady state strides of each experiment were selected, starting and ending with apex. One stride was defined to consist of stance and flight phase for one leg. The mean over the trial for both current and voltage was calculated. The electrical power results in

$$P_{el} = \tilde{U} \cdot \tilde{I}. \tag{5}$$

where $\tilde{U}$ and $\tilde{I}$ denote the average voltage and current over the trial respectively. The electrical cost of transport (CoT) is defined as

$$CoT_{el} = \frac{P_{el}}{m \cdot g \cdot \tilde{v}} \quad , \tag{6}$$

with m being the robot's mass, g being the gravitational acceleration and $\tilde{v}$ being the average forward velocity. The mechanical power generated for forward locomotion was derived from the calculated leg forces (F) and instantaneous velocity (v)

$$P_{mech} = \frac{1}{\sigma} \sum_{i=1}^{\sigma} F_i \cdot v_i \quad , \tag{7}$$

with s denoting the number of samples in a trial. The mechanical cost of transport was calculated accordingly

$$CoT_{mech} = \frac{P_{mech}}{m \cdot g \cdot \tilde{v}}. \tag{8}$$

For better comparison the Froude number, a dimensionless characteristic velocity was calculated as

$$F_r = \frac{\tilde{v}^2}{g \cdot l_0}. \tag{9}$$

III. Results

The robot has demonstrated dynamic gaits on compliant legs over a wide range of step length, and hip torques (Tab. III). Speeds between 0.5 m/s and 1 m/s were achieved at a

#	φ_{AEA} [rad]	φ_{PEA} [rad]	I_τ [A]	Stance l_{leg} [m]	Stance k_p [A/rad]	Stance k_d [As/rad]	Flight l_{leg} [m]	Flight k_p [A/rad]	Flight k_d [As/rad]
1	1.34	1.8	30	0.9	1500	20	0.65	200	10
2	1.34	1.74	30	0.9	1500	20	0.65	200	10
3	1.4	1.8	30	0.9	1500	20	0.65	200	10
4	1.34	1.74	40	0.9	1500	20	0.65	200	10
5	1.34	1.8	60	0.9	1500	20	0.65	200	10
6	1.38	1.8	40	0.9	1500	20	0.65	200	10
7	1.42	1.8	40	0.9	1500	20	0.65	200	10
8	1.4	1.85	45	0.9	2000	20	0.7	400	10
9	1.4	1.8	50	0.9	1500	20	0.65	200	10
10	1.4	1.8	50	0.9	1500	20	0.65	200	10
11	1.33	1.75	70	0.9	2000	20	0.7	200	10
drop	1.42	1.85	45	0.9	2000	20	0.65	200	10
outd.	1.4	1.85	45	0.9	2000	20	0.7	200	10

TABLE II: Control parameters for flat ground (1-11), drop, and outdoor experiments (outd.).

mechanical cost of transport between 0.1 and 1 (values for human walking are reported around 0.05 [36, Sec. III-A]). Generated force profiles indicate compliant leg operation and resembled force profiles observed in animal walking as well as the spring-mass model. The robot was able to exhibit grounded running, a hybrid gait with no aerial phases but typical running force profiles (Sec. III-B) that, to our knowledge, has not been reported for bipedal robot locomotion before. The robot succeeded to walk over stairs and negotiate a drop without controller adaptations (Sec. III-C). In an outdoor environment the robot was able to generate walking gaits without sensing the properties of the substrate (Sec. III-D).

A. General results

Parameter sets that resulted in steady walking gaits were considered for presentation in this article. Successful gaits were achieved in a range of 0.5 m/s to 1 m/s. Body support and propulsion was consistently achieved, leg recirculation resulted in smooth transitions from stance into flight and back. Although the robot did not sense ground contact, the compliant leg allowed for soft touch-down after it retracted as intended by the controller (Fig. 6). Speed and power consumption, both mechanical and electrical are reported in Tab. III.

For a representative trial (#9), the force peak observed during stance was 792 N, the cycle time from one touch-down (TD) to the next TD of the same leg was 893 ms, stance time of one leg took 566 ms resulting in a duty cycle of 0.63. The touch-down angle was fairly constant at $69.7°$ and the average walking speed was 0.84 m/s, resulting in a Froude number of 0.09.

#	v [m/s]	F_r [1]	P_m [W]	CoT_m [1]	P_e [W]	CoT_e [1]
1	0.53	0.03	145	0.49	392.8	1.31
2	0.53	0.03	135.7	0.45	408.8	1.35
3	0.58	0.04	130.1	0.40	423.8	1.29
4	0.61	0.04	174.7	0.51	481.2	1.40
5	0.63	0.05	205.7	0.57	540.3	1.51
6	0.68	0.05	167.8	0.43	546.3	1.41
7	0.68	0.05	118.4	0.31	504.3	1.31
8	0.83	0.08	70.7	0.14	503.4	1.06
9	0.84	0.09	98.0	0.20	515.2	1.08
10	0.93	0.1	209.6	0.40	618.3	1.17
11	0.99	0.12	54.0	0.10	547.1	0.97
drop	0.85	0.09	79.8	0.16	541.2	1.12
outd.	0.54	0.03	87.6	0.29	439.2	1.43

TABLE III: Experimental results for individual experiments, average speed (v), Froude number (F_r), mechanical power (P_m), mechanical cost of transport (CoT_m), electrical power (P_e) and electrical cost of transport (CoT_e).

B. Leg forces

Leg forces measured during steady state walking experiments are based on spring deflection and showed the characteristic, double-humped force profile during stance. Distinct double support phases were observed (Fig. 7). The maximum leg force during steady state walking was as high as 783 N $\pm$ 180 N and was similar in both legs. During swing phase, oscillations about the resting angle of the springs are observed. In trial 4 the robot settled into a dynamically different gait exhibiting single-humped force profiles with peaks of 941 N (Fig. 9) with clear double support phases. This gait called *grounded running* has been predicted by the spring mass model, and has been found in animal locomotion. The spring mass model predicted grounded running at the same energy levels as walking with slightly increased angles of attack [37]. The average angle of attack observed in this trial was 70.3^o. To our knowledge, this gait has not been observed in robots before. For both gaits the robot's CoM exhibited an oscillatory

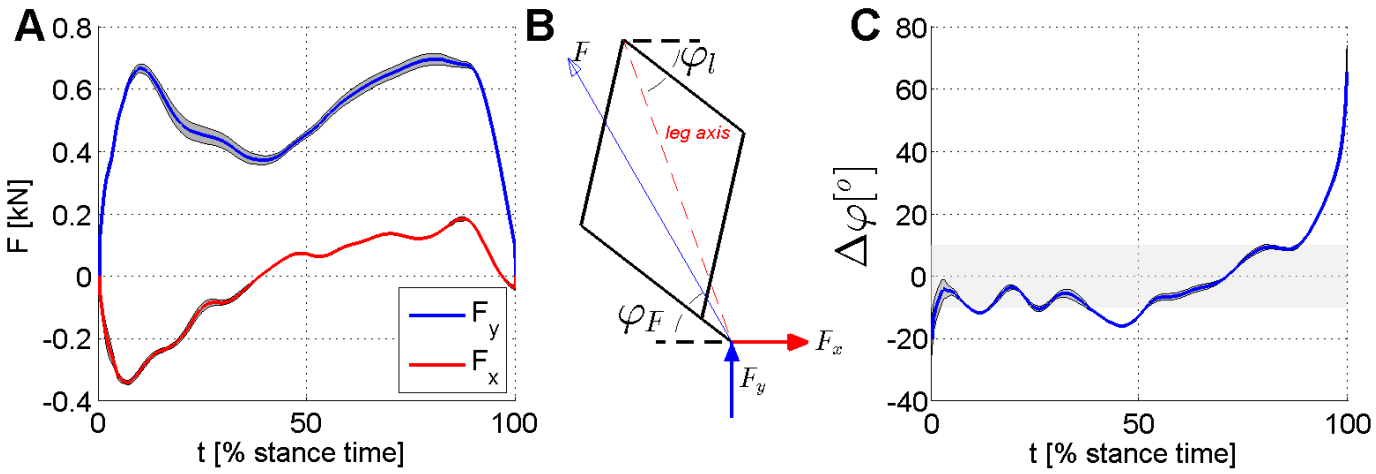

Fig. 8: Force profile and direction: Panel **A** shows the ground reaction forces in vertical (F_y) and horizontal (F_x) direction (for definition see Panel **B**) during stance. Panel **C** shows the average deviation from the leg axis in degrees during stance. The shaded grey area indicates a deviation of less than $10°$.

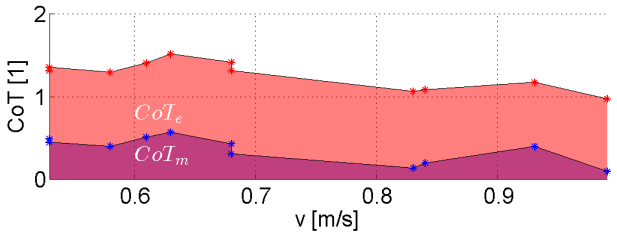

Fig. 5: Cost of transport plotted over forward speed. The dark patch represents the mechanical cost of transport, the lighter patch the electrical cost of transport. Measured data points (Table III) are indicated by * and * for electrical and mechanical CoT, respectively.

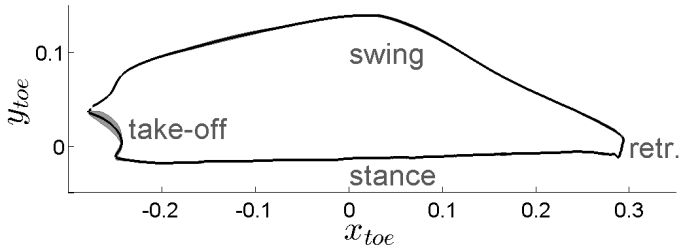

Fig. 6: Mean toe trajectory and standard deviation from 18 consecutive steps. The trajectory was calculated relative to the robot's CoM based on leg angle and length. Four distinct phases can be identified, i.e. stance, take-off, swing and leg retraction (retr.).

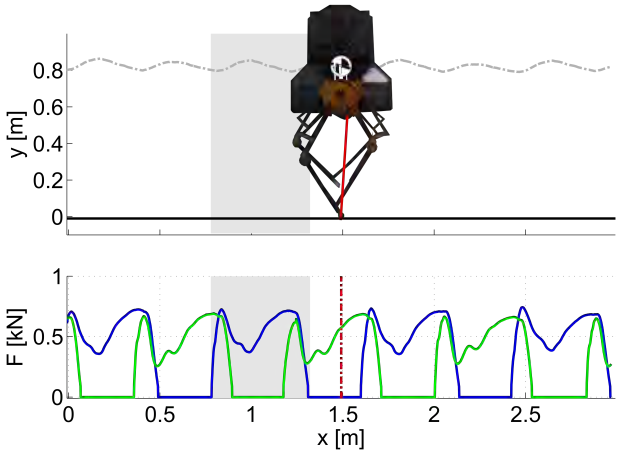

Fig. 7: Center of mass (CoM) motion (top panel) and leg forces (bottom panel) from experimental data for steady walking. Top panel: the robot's center of mass position is indicated above the leg motors, direction and magnitude of the instantaneous leg force for the stance leg is indicated by a red line. Bottom panel: axial leg force in kN is plotted over the robot's CoM position (indicated by dashed red line), the left leg's force is indicated in blue, the force of the right leg in green.

trajectory.

The tangential leg force caused by the generated hip torque is required to power the gait. This was found to lead to a deviation ($\Delta\varphi$) of leg axis and overall force of less than $10°$ for most of the gait cycle (Fig. 8C). The tangential leg force in average accounted for $0.6\pm19.3\,\%$ of the axial leg force over one stance phase. Despite this deviation from the template model the axial leg force accounts for the characteristic ground reaction forces as indicated by comparing Fig. 7 and Fig. 8A.

C. Step down experiments

The robot walked for several steps on flat ground to settle into a steady gait, then ascended steps of 2.1cm height and stepped down the drop. Leg forces show that it took two steps to recover from the drop and exhibit steady gait force patterns again (Fig. 10). Interestingly, the second step after the drop showed a clearly increased force peak. Steps and drops were traversed with an average speed of 0.84 m/s, the electrical cost of transport was slightly increased in comparison with a level

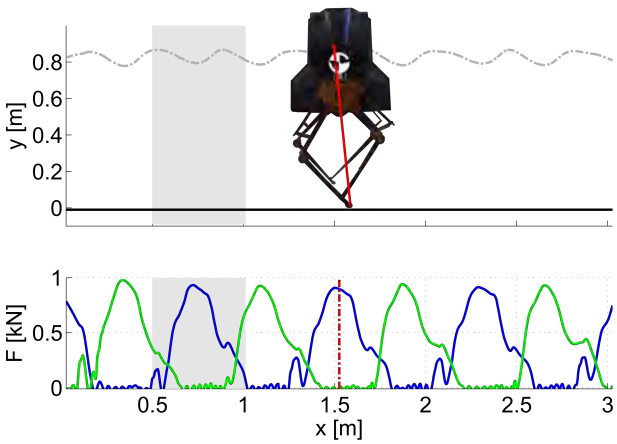

Fig. 9: Experimentally measured CoM trajectory and force profiles. The robot exhibited dynamics clearly different from walking trials (compare Fig. 7). Single humped force profile indicate running dynamics, though no aerial phases were observed. The dynamics of one stance phase are indicated by the shadowed area.

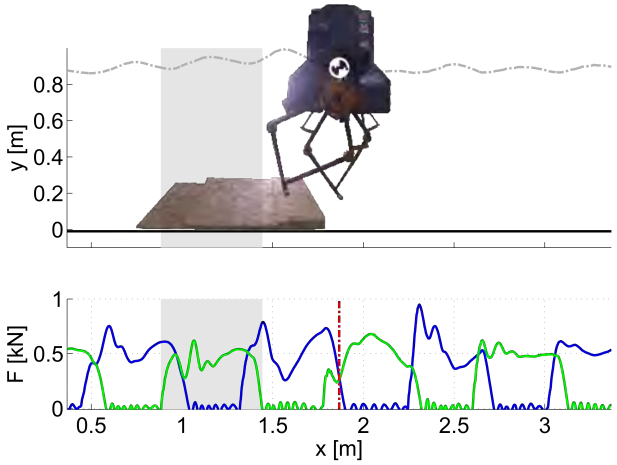

Fig. 10: Schematic and force traces of a drop step experiment. The robot ascended three steps and steps down the drop with the right leg (green force profile). Axial force profiles are plotted over CoM trajectory, in blue for the left leg, in green for the right leg. The robot steps on the first step with the right leg (green), ascends onto the second step with the left leg and hits the third step with the right leg again. The associated force profiles show increased peak-forces, as well as the forces of the two steps after the drop are increased. From the third step after dropping down, the force profiles return to steady state.

ground trial at the same speed, whereas the mechanical cost of transport showed a slight decrease (Tab. III).

D. Outdoor experiments

On unpredictable ground, the robot settled into a slow gait with clearly increased cost of transport (Tab. III). The robot walked continuously for more than 20 steps in several experiments. Although ground contact in terms of substrate position and rigidity was unpredictable, ensuring sufficient grip on the ground druing contact to generate propulsion was not a problem.

Fig. 11: *ATRIAS* walking outdoor on a plain, natural lawn.

	ATRIAS	human	*ASIMO*	*C. Ranger*
CoT_m	0.4 ± 0.26	0.05	1.6	0.055
CoT_e	1.3 ± 0.17	0.2	3.2	0.2

TABLE IV: Cost of transport references for human walking [36], the *ASIMO* humanoid and the *Cornell Ranger* [18]

IV. Discussion

The successful mechanical implementation of a biologically relevant template model for dynamic gaits in a full size bipedal robot marks a milestone in dynamic robotics developments. In our experiments we were able to demonstrate, that the passive compliance of the robot can be combined with actuation in a sensible way to facilitate sustainable, versatile locomotion.

The reproduction of typical GRFs observed in the spring-mass model for walking and running over a range of locomotion speeds indicate a dynamic match of model and robot. This lays the foundation for the application of control concepts proposed by studies of the spring mass model to negotiate different kinds of terrain and limit structural dynamic loads. Andrada, Nyakatura, Müller, *et al.* [38] pointed out the potential of grounded running as a fast and adaptable gait for robots, a fact that has been widely overlooked by roboticists. The grounded running observed in the experiments presented here consolidate the potential benefit of specifically designing the passive dynamics of a robot to facilitate gait versatility.

The demonstration of the robot's passive dynamics reproduced a number of model predictions. The leg compliance made the robot very robust to changes in terrain as shown in the drop step and outdoor experiments. The smooth swing to stance transition of the legs has been enabled by ground speed matching through leg retraction as proposed in [11].

Energy efficiency is one of the key factors required for locomoting machines, as they have to carry their source of energy. Different levels of autonomy, versatility and performance make it hard to directly compare robots. In our experiments the cost of transport varied with control parameters, indicating that some gaits match the robot's natural dynamics better than others. The achieved mechanical cost of transport of 0.4 ± 0.26 and electrical CoT of 1.26 ± 0.17 however indicate a high potential for efficient locomotion, advertising the use of compliant structures. For reference, human walking is reported to have a cost of transport of 0.05 (mech.) and 0.2 (metabolic).

In general we found that compliant legs remove the need to actively control the impact to avoid structural damage to the robot and therefore largely relaxes control. Furthermore, collisional losses are reduced by recovering kinetic energy from potential energy stored in the springs.
Considering the fact, that the majority of simulation studies assume a steady gait, the proposed controller constitutes a feasible way to settle into a steady gait from a standing position.

Comparison to natural systems

Template models like the spring mass model are often used to discover basic principles in animal locomotion. The declaratory nature of model findings not tested in the real world has been criticised in [39]. While the inverted pendulum found its real world representation in a number of robots, only few technical devices were engineered to reproduce spring mass dynamics, leaving a heap of model findings in the realms of simulation.
Recent experiments on birds negotiating obstacles lead to the conclusion that birds constrain peak leg forces in a drop step [40]. The force profile recorded in our experiments (Fig. 10) shows similar dynamics in the drop step, i.e. the peak force hits the same magnitude as in the steps before. Interestingly, the second step after the drop shows an increased peak and it takes until the third step to settle back into a steady gait indicating a wider time frame for drop negotiation dynamics. The successful deployment in a realistic outdoor environment of our robot that, to our knowledge, is not very common for modern bipeds, will further enhance the robot's capabilities to produce valuable insights into the applicability of simulation driven insights.

Next steps

The demonstrated dynamic capabilities open the doors for a number of control concepts to be implemented. The robot's ability to directly control the ground reaction forces based on measured spring deflection allows for a more rigorous enforcement of desired dynamics, i.e. matching particular gaits derived from the spring-mass-template. Control strategies developed based on computer simulations, e.g. swing leg policies for ground height disturbances proposed by [41], negotiation of compliant ground as described by [13] or strategies for trunk stabilisation [12], will be adapted for walking, implemented and tested.
Although the robot has been capable of hopping [30], insufficient electric power supply did prevent sustained running until now. New commercial amplifiers with higher power ratings will solve this shortcoming in the near future, adding to the dynamic capabilities of the robot.

In conclusion we identified a high potential in combining engineered passive dynamics and active control in a bipedal robot. The successful demonstration of dynamic matching between robot and template strongly accents the applicability of proposed control strategies .

ACKNOWLEDGMENT

The authors would like to thank Kit Morton, Ryan van Why, Michael Anderson, Soo-Hyun Yoo, Ryan Skeele, and Mikhail Jones for their respective contributions to the robot's control and data acquisition system and their support to execute the experiments.
The authors acknowledge our funding sources for this project: Defense Advanced Research Projects Agency (DARPA) grant #W91CRB-11-1-0002, Human Frontier Science Program (HFSP) grant #RGY0062/2010, and National Science Foundation (NSF) grant #1100232.

MULTIMEDIA

Videos and experimental data are available at http://daniel.human-motion-engineering.org/ATRIAS

REFERENCES

[1] R. Blickhan, A. Seyfarth, H. Geyer, S. Grimmer, H. Wagner, and M. Gunther, "Intelligence by mechanics," *Philosophical Transactions of the Royal Society A Mathematical Physical and Engineering Sciences*, vol. 365, no. 1850, pp. 199–220, 2007.
[2] T. McGeer, "Passive dynamic walking," *IJRR*, vol. 9, pp. 62–82, 1990.
[3] R. Blickhan, "The spring-mass model for running and hopping," *Journal of Biomechanics*, vol. 22, no. 11-12, pp. 1217–1227, 1989.
[4] H. Geyer, A. Seyfarth, and R. Blickhan, "Compliant leg behaviour explains basic dynamics of walking and running," *Proceedings of the Royal Society B Biological Sciences*, vol. 273, no. 1603, pp. 2861–2867, 2006.
[5] J. Schmitt and P. Holmes, "Mechanical models for insect locomotion: dynamics and stability in the horizontal plane-ii. application," *Biol. Cybern.*, vol. 83, no. 6, pp. 517–527, 2000.
[6] P. Holmes, R. J. Full, D. Koditschek, and J. Guckenheimer, "The dynamics of legged locomotion: models, analyses, and challenges," *Siam Rev.*, vol. 48, no. 2, pp. 207–304, 2006.
[7] I. Poulakakis and J. Grizzle, "The spring loaded inverted pendulum as the hybrid zero dynamics of an asymmetric hopper," *IEEE Transactions on Automatic Control*, vol. 54, no. 8, pp. 1779–1793, 2009.
[8] R. Altendorfer, U. Saranli, H. Komsuoglu, D. E. Koditschek, B. Brown, M. Buehler, E. Moore, D. McMordie, and R. J. Full, "Evidence for spring loaded inverted pendulum running in a hexapod robot," in *Experimental Robotics VII*, 2002.
[9] S. R. Bullimore and J. F. Burn, "Ability of the planar spring-mass model to predict mechanical parameters in running humans," *Journal of Theoretical Biology*, vol. 248, no. 4, pp. 686–695, 2007.
[10] S. W. Lipfert, M. Gnther, D. Renjewski, S. Grimmer, and A. Seyfarth, "A model-experiment comparison of system dynamics for human walking and running," *Journal of Theoretical Biology*, vol. 292, pp. 11–17, 2012.

[11] Y Blum, S. W. Lipfert, J Rummel, and A Seyfarth, "Swing leg control in human running," *Bioinspiration & Biomimetics*, vol. 5, no. 2, p. 026 006, 2010.

[12] H.-M. Maus, S. Lipfert, M. Gross, J. Rummel, and A. Seyfarth, "Upright human gait did not provide a major mechanical challenge for our ancestors," *Nature Communications*, vol. 1, no. 6, pp. 1–6, 2010.

[13] C. Hubicki and J. W. Hurst, "Running on soft ground: simple, energy-optimal disturbance rejection," in *CLAWAR 2012*, 2012, pp. 543–547.

[14] F. Peuker, C. Maufroy, and A. Seyfarth, "Leg-adjustment strategies for stable running in three dimensions," *Bioinspiration & Biomimetics*, vol. 7, no. 3, p. 036 002, 2012.

[15] M. H. Raibert, in *Legged Robots That Balance*. Cambridge: MIT Press, 1986.

[16] T. McGeer, "Passive dynamic walking," *Int. J. Robot. Res.*, vol. 9, pp. 62–82, 1990.

[17] S. H. Collins, "A three-dimensional passive-dynamic walking robot with two legs and knees," *The International Journal of Robotics Research*, vol. 20, no. 7, pp. 607–615, 2001.

[18] S. Collins, A. Ruina, R. Tedrake, and M. Wisse, "Efficient bipedal robots based on passive-dynamic walkers," *Science*, vol. 307, pp. 1082–1085, 2005.

[19] S. Kazuo, K. Tsuchiya, and K. Tsujita, "The intelligent ASIMO system overview and integration," in *ICRA*, New Orleans, LA, 2004, pp. 3043–3048.

[20] R. Tajima, D. Honda, and K. Suga, "Fast running experiments involving a humanoid robot," IEEE, 2009, pp. 1571–1576.

[21] K. Kaneko, F. Kanehiro, M. Morisawa, K. Akachi, G. Miyamori, A. Hayashi, and N. Kanehira, "Humanoid robot hrp-4-humanoid robotics platform with lightweight and slim body," in *Intelligent Robots and Systems (IROS), 2011 IEEE/RSJ International Conference on*, 2011, 44004407.

[22] J. E. Pratt and G. A. Pratt, "Exploiting natural dynamics in the control of a planar bipedal walking robot," in *Proceedings of the annual allerton conference on communication control and computing*, vol. 36, 1998, 739748.

[23] J. W. Grizzle, J. Hurst, B. Morris, H. W. Park, and K. Sreenath, "Mabel, a new robotic bipedal walker and runner," in *American Control Conference*, St. Louis, Jun. 2009.

[24] S. Hyon and T. Emura, "Symmetric walking control: invariance and global stability," in *Robotics and Automation, 2005. ICRA 2005. Proceedings of the 2005 IEEE International Conference on*, 2005, 14431450.

[25] M. Wisse and J. v. Frankenhuyzen, "Design and construction of mike: a 2d autonomous biped based on passive dynamic walking," presented at the, Kyoto, 2003.

[26] R. Niiyama, S. Nishikawa, and Y. Kuniyoshi, "Athlete robot with applied human muscle activation patterns for bipedal running," in *10th International Conference on Humanoid Robots*, 2010, 498503.

[27] K. Radkhah, D. Scholz, O. v. Stryk, M. Maus, and A. Seyfarth, "Towards human-like bipedal locomotion with three-segmented elastic legs," *Proc. ISR*, pp. 1–8, 2010.

[28] D. Renjewski, "An engineering contribution to human gait biomechanics," Dissertation, TU Ilmenau, Germany, 2012.

[29] E. Andrada, J. A. Nyakatura, F. Bergmann, and R. Blickhan, "Adjustments of global and local hindlimb properties during terrestrial locomotion of the common quail (coturnix coturnix)," *Journal of Experimental Biology*, vol. 216, no. 20, pp. 3906–3916, 2013.

[30] C. Hubicki, J. Grimes, M. Jones, D. Renjewski, A. Sprwitz, A. Abate, and J. Hurst, "ATRIAS: enabling agile biped locomotion with a template-driven approach to robot design," *IJRR (submitted)*, 2013.

[31] J. S. Collett and J. W. Hurst, "Artificial restraint systems for walking and running robots: an overview," *International Journal of Humanoid Robotics*, vol. 09, no. 01, p. 1 250 001, 2012.

[32] U. Saranli, M. Buehler, and D. Koditschek, "Design, modeling and preliminary control of a compliant hexapod robot," in *Robotics and Automation, 2000. Proceedings. ICRA '00. IEEE International Conference on*, vol. 3, 2000, pp. 2589–2596.

[33] A. Sprowitz, A. Tuleu, M. Vespignani, M. Ajallooeian, E. Badri, and A. J. Ijspeert, "Towards dynamic trot gait locomotion: design, control, and experiments with cheetah-cub, a compliant quadruped robot," *The International Journal of Robotics Research*, vol. 32, no. 8, pp. 932–950, 2013.

[34] J. Pratt, P. Dilworth, and G. Pratt, "Virtual model control of a bipedal walking robot," in *ICRA97*, Apr. 1997, pp. 193–198.

[35] A. Peekema, D. Renjewski, and J. W. Hurst, "Open-source real-time robot operation and control system for highly dynamic, modular machines," in *ASME 2013, International Design Engineering Technical Conferences & International Conference on Multibody Systems, Nonlinear Dynamics, and Control*, 2013.

[36] N. H. Molen, R. H. Rozendal, and W. Boon, "Graphic representation of the relationship between oxygen-consumption and characteristics of normal gait of the human male.," *Proceedings of the Koninklijke Nederlandse Akademie van Wetenschappen. Series C. Biological and medical sciences*, vol. 75, no. 4, p. 305, 1972.

[37] J. Rummel, Y. Blum, and A. Seyfarth, "From walking to running," in *Autonome Mobile Systeme 2009*, R. Dillmann, J. Beyerer, C. Stiller, J. M. Zllner, and T. Gindele, Eds., ser. Informatik aktuell, Springer Berlin Heidelberg, 2009, pp. 89–96.

[38] E. Andrada, J. Nyakatura, R. Müller, C. Rode, and R. Blickhan, "Grounded running: an overlooked strategy for robots," *Autonomous Mobile Systems 2012*, 7987, 2012.

[39] K. T. Kalveram and A. Seyfarth, "Inverse biomimetics: how robots can help to verify concepts concerning sensorimotor control of human arm and leg move-

ments," *Journal of Physiology-Paris*, vol. 103, no. 3-5, pp. 232–243, 2009.

[40] A. Birn-Jeffery, C. Hubicki, Y. Blum, D. Renjewski, J. Hurst, and M. Daley, "Dont break a leg: running birds prioritise safety and economy, not strict stability," *Journal of Experimental Biology (submitted)*, 2014.

[41] H. R. Vejdani, Y Blum, M. A. Daley, and J. W. Hurst, "Bio-inspired swing leg control for spring-mass robots running on ground with unexpected height disturbance," *Bioinspiration & Biomimetics*, vol. 8, no. 4, p. 046 006, 2013.

Daniel Renjewski is a Postdoctoral Researcher at the Dynamic Robotics Laboratory, at Oregon State University. He received his Diploma in Engineering degree in biomechatronics (Dipl.-Ing.), and his doctorate in engineering (Dr.-Ing.), from Ilmenau University of Technology in 2007, and 2012. His research interests include human gait biomechanics, legged robotics and bioinspired control for legged locomotion.

Alexander Spröwitz is a Postdoctoral Researcher, currently working at the Royal Veterinary College, London. He has a B.S. in Mechanical Engineering, a Diplom in Biomechatronics from Ilmenau University, Germany, and a Ph.D. in Manufacturing Systems and Robotics from EPFL, Switzerland. His research include self-reconfiguring modular robots, bipedal and quadrupedal legged robots, and biomechanics of legged robotic and animal locomotion, such as in running birds.

Jonathan Hurst is an Assistant Professor of Mechanical Engineering, and Director of the Dynamic Robotics Laboratory, at Oregon State University. He received the B.S. degree in mechanical engineering, and an M.S. and Ph.D. in robotics, from Carnegie Mellon University in 2001, 2004 and 2008. His research interests include integrated mechanical design and control for legged locomotion, with a focus on the role of natural dynamics.